Shear stress affects the intracellular distribution of eNOS: direct demonstration by a novel in vivo technique

Caroline Cheng, Rien van Haperen, Monique de Waard, Luc C. A. van Damme, Dennie Tempel, Laurens Hanemaaijer, Gert W. A. van Cappellen, Joop Bos, Cornelis J. Slager, Dirk J. Duncker, Anton F. W. van der Steen, Rini de Crom, and Rob Krams

The focal location of atherosclerosis in the vascular tree is correlated with local variations in shear stress. We developed a method to induce defined variations in shear stress in a straight vessel segment of a mouse. To this end, a cylinder with a tapered lumen was placed around the carotid artery, inducing a high shear stress field. Concomitantly, regions of low shear stress and oscillatory shear stress were created upstream and downstream of the device, respectively. This device was used in mice transgenic for an *eNOS3GFP* fusion gene. We observed a strong induction of endothelial nitric oxide synthase–green fluorescent protein (eNOS-GFP) mRNA expression in the high shear stress region compared with the other regions ($P < .05$). Quantification of eNOS-GFP fluorescence or of immunoreactivity to the Golgi complex or to platelet endothelial cell adhesion molecule 1 (PECAM-1) showed an increase in the high shear stress region ($P < .05$) compared with nontreated carotid arteries. Colocalization of eNOS-GFP with either the Golgi complex or PECAM-1 also responded to alterations of shear stress. In conclusion, we showed a direct response of mRNA and protein expression in vivo to induced variations of shear stress. This model provides the opportunity to study the relationship between shear stress alterations, gene expression, and atherosclerosis. (Blood. 2005;106:3691-3698)

Introduction

Wall shear stress is the drag force acting on the endothelial cells as a result of the blood flow. In straight arteries, laminar flow with an average shear stress level of 1.5 N/m^2 prevails and this level is actively maintained by adjusting the vascular tone and by structural remodelling in response to shear stress.[1,2]

The relationship between low wall shear stress and the occurrence of atherosclerotic lesions in the vascular tree has been recognized for several decades,[3,4] but the mechanism underlying this relationship is unknown. Furthermore, it is not clear whether low shear stress (< 1.5 N/m^2) or oscillatory shear stress (exhibiting directional change) is more important for the development of atherosclerosis.[5,6] It has been postulated that altered shear stress results in changes in gene expression and protein function.[7,8] This was confirmed in experiments studying endothelial cells in flow chambers under well-controlled shear stress conditions in vitro.[9,10] Such changes can underlie the observed susceptibility to atherosclerosis of the affected vascular regions. Indeed, endothelial cells located at atherosclerosis-susceptible sites show a specific pattern of gene expression in vivo,[11,12] indicating a relationship with shear stress. However, this relationship has not been substantiated by direct causal in vivo evidence. Moreover, there is no in vivo model that generates oscillations in shear stress. Therefore, we developed a new method by which low and oscillatory shear stress is introduced in different segments of a straight vessel. The first aim of the present study is to demonstrate that the proposed method induces a complex shear stress field in vivo.

To evaluate whether these changes in shear stress affect gene expression, we monitored one of the best-characterized shear stress responsive genes, endothelial nitric oxide synthase (*eNOS*).[13,14] This was studied in an in-house developed transgenic mouse model in which eNOS expression and distribution can be easily monitored by virtue of a fusion of the protein with green fluorescent protein (GFP).[15] The second aim is to study the effects of shear stress on the intracellular distribution of eNOS.

Regulation of eNOS protein levels and activity is unusually complex and occurs both at transcriptional and posttranscriptional levels.[16,17] Posttranslational modification of eNOS by myristoylation and palmitoylation that targets the protein to the Golgi complex and to the lipid-rich domains of the cell membrane are both necessary for proper eNOS activation. Shear stress activates eNOS predominantly through Akt-dependent phosphorylation of eNOS at serine 1177.[18,19] Recently, it was shown that the fraction of eNOS localized in the Golgi complex is responsive to phosphorylation by Akt.[20] This implies that shear stress activates eNOS when it is located in certain compartments of the endothelial cells. At present, it is unknown how shear stress affects the intracellular distribution of eNOS in vivo.[21] Therefore, we developed quantitative methods to analyze the intracellular distribution of eNOS in vessel regions exposed to different shear stress patterns in relation to the serine 1177 phosphorylation of eNOS.

From the Departments of Cardiology, Thoraxcenter, Cell Biology and Genetics, Development and Reproduction, Experimental Medical Instrumentation, and Vascular Surgery, Erasmus University Medical Center, Rotterdam, The Netherlands.

Submitted June 14, 2005; accepted July 22, 2005. Prepublished online as *Blood* First Edition Paper, August 16, 2005; DOI 10.1182/blood-2005-06-2326.

Supported by the Netherlands Heart Foundation (NHS), grant 2002T45, and the Interuniversity Cardiology Institute of the Netherlands (ICIN), project 33.

An Inside *Blood* analysis of this article appears in the front of this issue.

Reprints: Rob Krams, Erasmus MC, Rm Ee2216, Dr Molewaterplein 50 3015 GD Rotterdam, The Netherlands; e-mail: r.krams@erasmusmc.nl.

The publication costs of this article were defrayed in part by page charge payment. Therefore, and solely to indicate this fact, this article is hereby marked "advertisement" in accordance with 18 U.S.C. section 1734.

Materials and methods

Animals

Mice expressing an eNOS-GFP fusion protein were generated as described before.[15] Mice were bred to C57BL/6 background for at least 10 generations (> 99% C57BL/6) and were 15 to 20 weeks of age. Animal care and experiments complied with institutional and national guidelines.

In vivo alteration of shear stress

To induce standardized changes in shear stress, we designed a shear stress modifier, which was manufactured from the thermoplastic, polyetherketon. The device is referred to as "cast" throughout the study. The cast consists of 2 longitudinal halves of a cylinder with a cone-shaped lumen (Figure 1A). The geometry of the cast has been designed with computational flow dynamics software[22] (Sepran; Sepra, Delft, The Netherlands) to produce vortices downstream of the cast when placed around the common carotid artery (Figure 1B). This downstream region will therefore be exposed to oscillations in shear stress (oscillatory shear stress region). The upstream inner diameter is 500 μm (nonconstrictive) and gradually declines to 250 μm at the downstream side of the cast (constrictive). This tapering induces a gradual increase in shear stress (high shear stress region). In addition, the constrictive stenosis decreases the blood flow, resulting in a low shear stress region upstream from the cast. Control casts consist of a cylinder with a continuous nonconstrictive diameter of 500 μm. Adequacy of the cast design was evaluated by Doppler measurements.

For surgery, the mice were anesthetized with isoflurane. Both halves of the cast were placed around the right common carotid artery and fixed with a suture. Animals with cast implants were humanely killed at 1 to 6 days after surgery by in situ fixation.

Doppler measurements in mice

Mice were anesthetized with isoflurane, intubated, and ventilated with a 1:2 mixture of O_2/N_2O to which 2.3% isoflurane was added. The animals were maintained at 37°C on a heating-pad during the whole experiment; a neck incision was made and both the left and right common carotid arteries were dissected from connective tissue. Calibrated digital images were taken to measure vessel diameters. Doppler velocity signals were measured on both carotid arteries using a 20-MHz range-gated Doppler probe at a 45° angle from the vessel wall. The cast was then placed around the carotid artery upstream of the Doppler probe, and the measurement was repeated. Additionally, the Doppler signal in the left carotid artery after cast placement was recorded.

Doppler measurements in rabbits

Two groups of rabbits were studied. In the first group (n = 5), the immediate effect of cast placement was studied, whereas in the second group (n = 5) the chronic effect of a 2-week period of cast placement was evaluated. The rabbits were premedicated with a mixture of fentanyl (0.3 mg/mL) and fluanisone (0.6 mg/mL) and anesthetized with an infusion of fentanyl (infusion rate: 0.3 mg/kg/h) and a 2:1 mixture of N_2O and O_2. Subsequently, the rabbits were intubated and the respirator (Infant Respirator, Hoek Loos, Schiedam, The Netherlands) was adjusted to achieve and maintain physiologic blood gas levels (pH = 7.35-7.45; pCO_2 = 35-45 mm Hg; pO_2 > 100 mm Hg). The marginal ear artery was cannulated for arterial pressure measurement with a fluid-filled catheter (Amatek, Paoli, PA) for arterial blood withdrawal and for the infusion of fentanyl. During instrumentation of group 1 and after 2 weeks in group 2, the iliac artery was dissected and a 4 French sheet (Fast Cath; Daig, Minnetonka, MN) was placed for the advancement of guide wires and guiding catheters. Subsequently, the carotid artery was surgically exposed and dissected from its surrounding tissue. As a next step, in both groups, one of the carotid arteries was dissected and a 20-mHz range-gated Doppler sensor (model VF-1; Crystal Biotech, Hopkinton, MA) was placed at an angle of 45°. The range-gating properties allowed us to determine minimal and maximal velocities across the vessel lumen. The other carotid artery was used as a control vessel. Then the cast was placed around the carotid artery and recordings of systemic hemodynamics and Doppler velocities downstream of the cast were repeated. The Doppler measurements distally from the cast were used for the detection of velocity reversal. To that end, we carefully positioned the Doppler sensor to place the sample volume near the expected location of the vortex. All experiments were performed in accordance with the "Guiding Principles for the Care and Use of Animals" as approved by the Council of the American Physiological Society.

Confocal microscopy

Tissue samples were examined under a Zeiss LSM510LNO inverted laser scanning confocal fluorescence microscope (Carl Zeiss, Thornwood, NY). Images of GFP fluorescence were acquired by excitation with a 488-nm argon laser and were detected using a 500- to 550-nm band pass barrier filter. Background fluorescence was corrected by subtracting the image that was acquired after filtering the emission spectrum with a 560-nm long pass filter. To obtain an image of an intact whole mounted vessel, an optical slice of 40 μm thickness and 500 × 500 μm in cross-sectional area was obtained using a 10 ×/0.3 Axiovert lens. Next, the position of the table was changed to image several adjacent vessel sections encompassing the entire vessel segment under study. Individual images were fused to form a tile

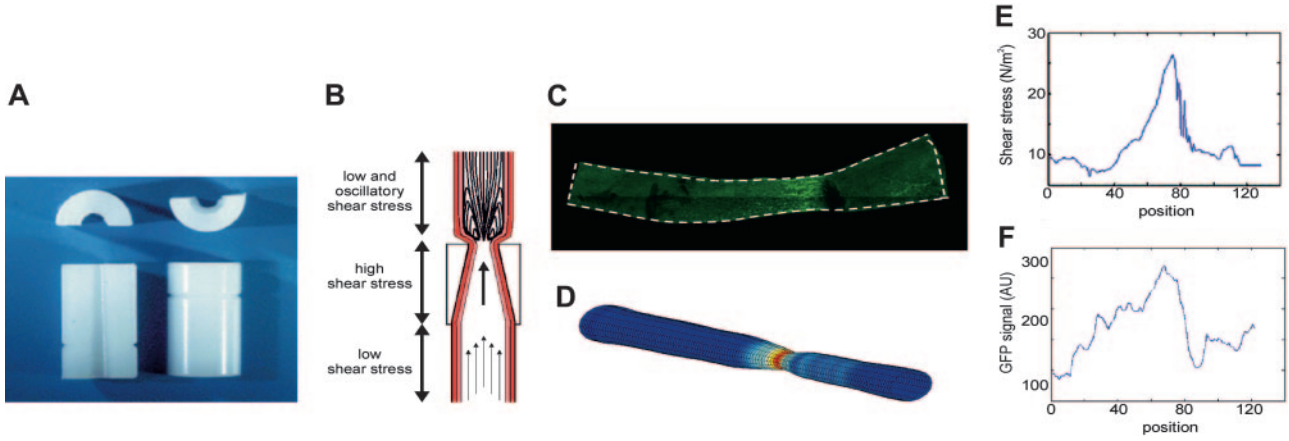

Figure 1. Design of the shear stress modifier: cast model. (A) The cast consists of 2 longitudinal halves of a cylinder with a conical lumen. (B) The theoretical design with induction of large vortices downstream of the cast in the carotid artery. Additionally, the conical lumen induces a stenosis of the vessel, causing a gradual increase in vascular shear stress in the cast area. Because of the stenosis, a region of low shear stress is created upstream of the cast. (C) Contours were obtained of GFP images, assuming a circular geometry of the vessel. (D) The computer generated 3-dimensional mesh of the vessel lumen in which the shear stress was calculated. (E) The distribution of shear stress (N/m^2) along the vessel. (F) Quantification of the GFP signal using the same images as used for shear stress calculations. The distribution of eNOS-GFP (in arbitrary units) is given along the vessel wall.

(Figure 1D) to provide a complete picture of the vessel. To study eNOS-GFP expression on a cellular level, stacks of optical slices ($0.5 \times 20 \times 20$ μm) were obtained using a 40 ×/1.2 water-immersion Axiovert lens. To investigate the location of serine 1177–phosphorylated eNOS, platelet endothelial cell adhesion molecule 1 (PECAM-1) and the Golgi complex, images of rhodamine fluorescence were taken applying a 543-nm excitation from a NeHe laser, using a 560-nm long pass filter for detection.

Fluorescence immunohistochemistry

Following in situ perfusion and overnight fixation, common carotid arteries were washed in phosphate-buffered saline (PBS) and treated with 0.2% Triton X-100 (Sigma Chemical, Zwijndrecht, The Netherlands) in PBS. The arteries were subsequently incubated with 2.5% horse serum in PBS/0.2% bovine serum albumin (BSA) for 30 minutes, washed again in PBS/0.2% BSA, and incubated with rabbit polyclonal antibodies against phospho-eNOS (serine 1177; New England Biolabs, Leusden, The Netherlands), PECAM-1 (Sigma Chemical), or mouse monoclonal antibodies against P115 (BD Biosciences PharMingen, San Diego, CA) in PBS/0.2% BSA overnight at 4°C. After washing in PBS/0.05% Tween-20 (Sigma Chemical), the arteries were incubated with mouse anti–rabbit IgG conjugated to R594 (Molecular Probes, Leiden, The Netherlands) or goat anti–mouse IgG conjugated to Texas red (Molecular Probes) in PBS/0.2% BSA for 2 hours at room temperature, followed by wash steps and were mounted in Vectashield (Vector Laboratories, Burlingame, CA).

Quantitative PCR

Carotid arteries treated with casts were divided into 3 different regions: 1 mm of the low shear stress region immediately upstream of the cast, 1 mm of the high shear stress region in the cast, and 1 mm of the oscillatory shear stress region immediately downstream of the cast. Similar 1-mm sections of the untreated contralateral carotid arteries from the same animals were isolated to serve as controls. Total RNA from each region was obtained using the RNAeasy kit (Qiagen, Cologne, Germany) and treated with DNase. cDNA was obtained by a reverse transcriptase reaction. Tissue samples of each region from 5 individual mice were pooled and human eNOS mRNA expression levels were analyzed by real-time polymerase chain reaction (PCR) using the iCycler iQ Detection System (Biorad, Veenendaal, The Netherlands) in 3 separate experiments. Specific primers for either human or mouse eNOS were used (primer sequences available on request). The hypoxanthine guanine phosphoribosyl transferase *(Hprt)* gene was used as a housekeeping gene.

Computational fluid dynamics

To estimate the augmentation in wall shear stress distribution after cast placement, a 3-dimensional computational fluid dynamic (CFD) technique was used.[22] The CFD needed the vessel geometry as input, which was obtained from the contours of the GFP images, assuming a circular geometry and constant circumference of the intact vessel (Figure 1C). On the basis of this geometry, a mesh was generated, which consisted of approximately 20 000 nodes. The boundary conditions for the calculations were no slip conditions at the wall, stationary parabolic inflow at the entrance with a maximal velocity equivalent to a shear stress of 1.5 N/m^2, and zero stress outflow. The combination of the mesh geometry and boundary conditions was used to solve the Navier-Stokes equations, applying a well-validated finite element software package (Sepran; Sepra, Delft, The Netherlands) to calculate shear stress (Figure 1D-E). The accuracy of the calculations was set at 10^{-4} m/s, which resulted in a numerical error of wall shear stress of approximately 1%.

Analysis and statistics

To relate the GFP signal to the shear stress calculations, the in-house developed software automatically selected the same region as used for the CFD analyses. The center line of the vessel was generated using an iterative optimization method. Lines of integration perpendicular to this center line served to average the GFP signal at similar positions as the shear stress calculations (Figure 1F). The relationship between shear stress and eNOS-GFP was described for each individual vessel by a sigmoid curve, applying an iterative algorithm. After setting initial parameters, an optimal data set was selected on the basis of a line search algorithm and a steepest decline algorithm.

Localization was quantified as percentage of the total image area. Colocalization of eNOS with the Golgi complex or with the plasma membrane compartment was quantified as percentage colocalization area of the total eNOS area. In addition, phospho-eNOS was expressed in percentages of total eNOS. All software was developed in Matlab (The Mathworks, Delft, The Netherlands). All regression analyses were performed by a commercial package (SigmaStat, version 2.03; Systat Software, Richmond, CA). Statistical analyses were performed using one-way ANOVA followed by the Dunnett ad-hoc test. The Student *t* test was used in the Doppler evaluations. Data are presented as mean plus or minus SEM. *P* values less than or equal to .05 were considered statistically significant.

Results

Evaluation of shear stress induction in vivo

Cast placement in rabbits induces flow reversal in the distal region. In a group of 10 New Zealand white rabbits, mean arterial blood pressure and heart rate were not affected, immediately and 2 weeks after cast placement. Average, maximal, and minimal Doppler velocities were consistent with a laminar velocity profile before cast placement. However, after cast placement all animals exhibited reversal of velocity near the endothelium distal from the cast with an unchanged maximal velocity in the center of the blood vessel (Table 1). These reversals in velocity indicate the occurrence of vortices in the area downstream from the cast.

Cast placement reduces the blood flow in the proximal region. In a group of eNOS-GFP transgenic mice, the average blood flow was initially 2.9 ± 0.3 mL/min and 2.8 ± 0.2 mL/min in the right and left common carotid arteries, respectively. Directly after cast placement, the blood flow was significantly reduced to an average of 2.0 ± 0.2 mL/min ($P < .001$) in the low shear stress region upstream of the cast in the right carotid artery. This reduction was observed in each animal. The reduction in blood flow was solely due to the increase in resistance from the stenosis caused by the cast because vascular diameters upstream of the cast region before (538 ± 39 μm) and immediately after (535 ± 48 μm) cast placement remained unchanged. The vascular diameter downstream of the cast region also remained unchanged after cast placement (546 ± 48 μm versus 593 ± 91 μm, respectively). In the left carotid artery, the blood flow was not affected by cast placement around the right vessel (2.75 ± 0.21 mL/min versus 2.88 ± 0.18 mL/min, respectively). Placement of a nontapering control cast around the right carotid artery did not affect the blood flow in both carotid arteries. Vascular remodelling of the carotid artery was

Table 1. Systemic hemodynamics before and after cast placement in 10 rabbits

	Before cast placement	After cast placement	Follow-up at 2 wk
Heart rate, bpm	200 ± 13	200 ± 12.5	196 ± 9.8
Mean arterial pressure, mm Hg	77 ± 1.8	73 ± 3.6	67 ± 2.2
Minimal velocity, cm/s	9.8 ± 2.5	−9.9 ± 1.9*	−10.4 ± 2.8*
Maximal velocity, cm/s	45.5 ± 10.7	37.1 ± 8.3	39.0 ± 14

*$P < .05$ versus before cast placement.

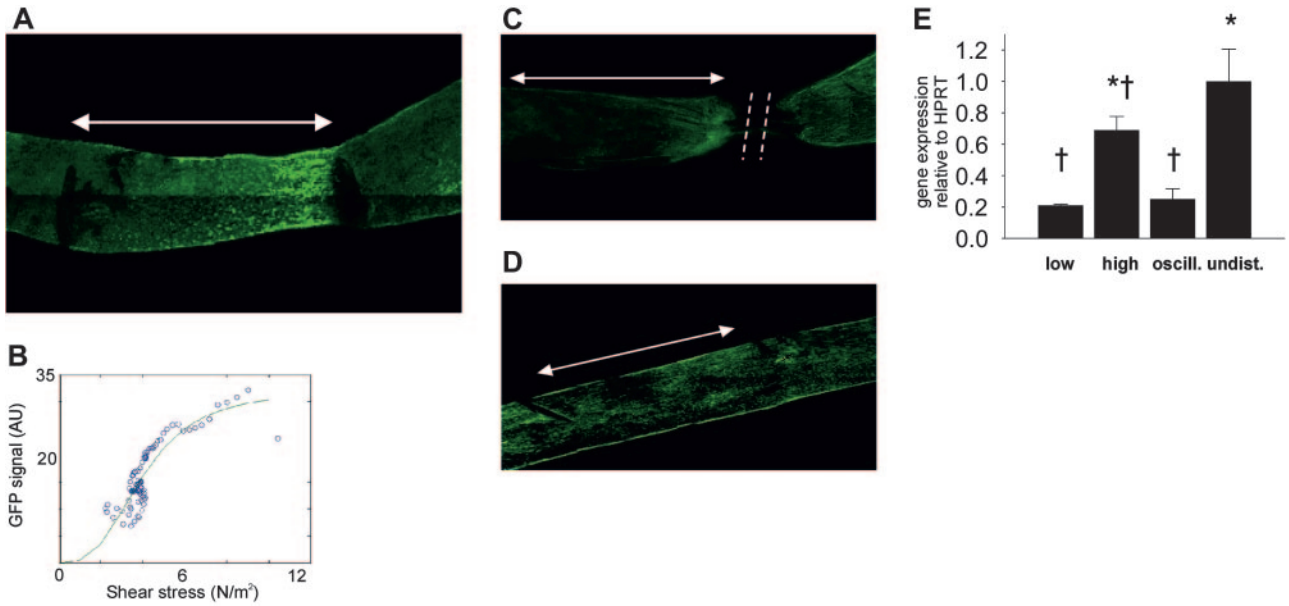

Figure 2. Effect of cast placement around carotid arteries on eNOS-GFP fluorescence. (A) Fluorescence of eNOS-GFP was imaged in the right carotid artery after the installation of a tapering cast (dashed line). The arrow indicates the position where the cast was situated (high shear stress region). The direction of the blood flow was from left to right. (B) Relationship between shear stress and eNOS-GFP fluorescence. Representative example of the relationship between the calculated shear stress and eNOS-GFP fluorescence along a linear segment of the carotid artery of an individual mouse. (C) Effect on eNOS-GFP fluorescence following downstream ligation of the carotid artery with a tapering cast or (D) placement of a nontapering cast. Arrows indicate the cast region, and dashed lines mark the site of ligation. (E) eNOS mRNA levels of the human transgene in the segments of the right carotid artery after the installment of a tapering cast: 1 mm immediately upstream of the cast (low shear stress), 1 mm in the cast (high shear stress), and 1 mm immediately downstream of the cast (oscillating shear stress), and in 1 mm of the contralateral control carotid artery (undisturbed shear stress); n = 3 groups (5 animals/group), $*P < .05$ versus low shear stress, $\dagger P < .05$ versus undisturbed shear stress. All data are means ± SEM. Note that panel A is derived from the same picture as that in Figure 1C.

minimal both in the upstream and downstream segments during the time period used in this study (6 days; data not shown).

Expression of eNOS protein is responsive to shear stress in vivo. In mice instrumented with the cast, a gradual increase in fluorescence is clearly visible along the length of the vessel segment that was located in the cast (Figure 2A, arrow). Both the fluorescent signal and the shear stress were quantified along the length of the carotid artery segment and were found to increase along the decreasing diameter of the cast (Figure 2B). Similar responses were observed in all of the treated animals. In a time series of 1, 2, 4, and 6 days of cast implantation, the response is already present after 1 day and remains unchanged for at least 6 days (data not shown). To exclude other factors introduced by tapering (eg, damage to the vessel wall and endothelium), control experiments were performed in which the blood vessel was ligated downstream of the cast, resulting in complete obstruction of the flow and consequently in the abolishment of shear stress. In this situation, the cast model does not induce variations in eNOS-GFP expression (Figure 2C), indicating that there are no direct effects of the surgical procedure or the presence of the cast. In addition, placement of the nonconstrictive control cast does not result in changes in eNOS-GFP expression (Figure 2D), indicating that the geometry of the constrictive cast, inducing variations in shear stress patterns, is responsible for the observed effects.

Next we assessed whether shear stress affects mRNA expression of the human eNOS transgene in the different regions. Both the low and oscillatory shear stress regions show a 3-fold decrease in eNOS mRNA expression compared with the control vessel (undisturbed shear stress; Figure 2E), whereas the average eNOS expression in the high shear stress region is similar to the control. The expression of endogenous murine eNOS was similarly affected by shear stress variations.

Shear stress affects intracellular distribution and activation of eNOS in vivo

Shear stress alters the intracellular distribution of eNOS. We compared the intracellular distribution of eNOS-GFP in the regions with different shear stress patterns. Endothelial cells in low, high, and undisturbed shear stress regions are elongated in shape and are aligned with the direction of the flow. In contrast, endothelial cells in the oscillatory shear stress region appear disorganized (middle panels in Figures 3A and 4A). At the intracellular level, eNOS-GFP is mainly located at a perinuclear site where the Golgi complex is situated, and it is present at the plasma membrane (Figure 3A, undisturbed shear stress). We investigated whether shear stress has an effect on the localization of eNOS-GFP protein in the Golgi complex by *en face* immunostaining (Figure 3A). Quantification of the fluorescent signal showed a 3-fold increase in the Golgi complex area in the vessel segment with high shear stress compared with undisturbed shear stress or low shear stress (Figure 3B). The eNOS-GFP area was increased by 8-fold and 7-fold in high shear stress and oscillatory shear stress, respectively, compared with either low or undisturbed shear stress (Figure 3C). High and oscillatory shear stress decreases the localization of eNOS in the Golgi complex by approximately 2-fold compared with undisturbed shear stress (Figure 3D). The difference in colocalization in the low shear stress area did not reach statistical significance.

We also studied the effect of shear stress on the localization of eNOS at the cell membrane by *en face* immunohistochemistry using a PECAM-1 antibody (Figure 4A). A 2-fold increase in PECAM-1 was observed in the high shear stress region (Figure 4B). The response of eNOS-GFP to the different shear stress fields was as observed before (Figures 3C and 4C). More eNOS

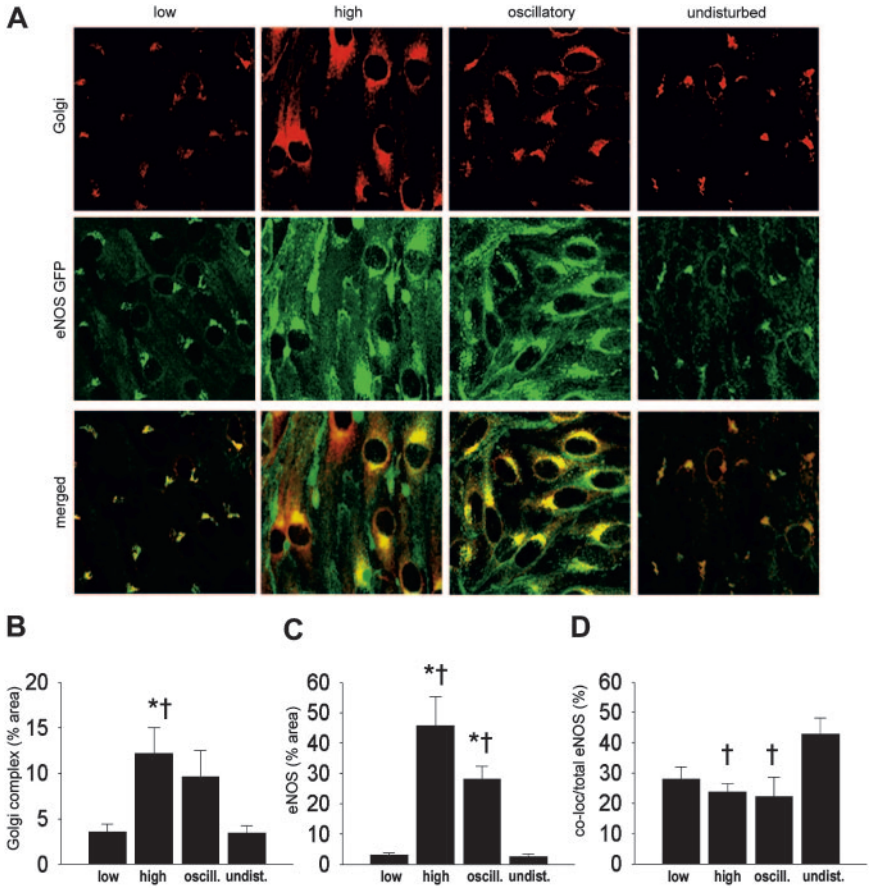

Figure 3. Intracellular localization of eNOS-GFP and Golgi complex in areas of the carotid artery experiencing different shear stress patterns after 2 days of cast placement. (A) In the top panel, Golgi complex in corresponding vascular regions visualized by *en face* immunofluorescence staining. Indicated are the low shear stress region (low), the high shear stress region (high), the oscillatory shear stress region (oscillatory), and the control region (undisturbed). Fluorescence was monitored by *en face* confocal microscopy in stacks of 500 × 500 × 40 μm each. In the middle panel, fluorescence of eNOS-GFP in endothelial cells located in the 3 different shear stress regions and in the contralateral carotid artery. In the bottom panel the top and middle panels are merged, showing the colocalization signal in yellow. (B-D) Quantification of the localization of (B) the Golgi complex, (C) the eNOS-GFP, and (D) the colocalization signals in response to the different shear stress fields in percentages of the total area (B-C) or of the total eNOS-GFP signal (D); n = 4, $*P < .05$ versus low shear stress. $\dagger P < .05$ versus undisturbed shear stress. All data are means ± SEM.

colocalized with PECAM-1 in the low and high shear stress region compared with the oscillatory shear stress region (2.5-fold difference; Figure 4D). A statistically significant correlation was found between the eNOS area and the Golgi complex area (Figure 5).

Shear stress effects on eNOS phosphorylation. To investigate whether shear stress has an effect on the phosphorylation of eNOS, *en face* immunostaining on carotid arteries was performed with antibodies against phospho-eNOS (serine 1177; Figure 6A). An increase in phospho-eNOS was observed in the high shear stress region compared with regions of low or undisturbed shear stress (6-fold), and oscillatory shear stress (2-fold; Figure 6B). Phospho-eNOS was also increased in the oscillatory shear stress area compared with regions of low or undisturbed shear stress (5-fold; Figure 6B). The eNOS-GFP response is similar to the results obtained before (Figure 6C). The fraction of eNOS that was phosphorylated, approximately 50%, did not change by alterations in shear stress (Figure 6D).

Discussion

In the present study, we describe a novel technique to induce complex shear stress fields in vivo. From the results, we conclude that (1) the technique induces changes in shear stress; (2) augmentation of shear stress results in elevated *NOS3* gene expression and eNOS protein levels as previously suggested by in vitro experiments; (3) intracellular distribution and phosphorylation of eNOS is responsive to high and oscillatory shear in vivo; and (4) these shear stress conditions result in eNOS redistribution with a relatively lower association to the Golgi complex. However, the fraction of eNOS that is activated by serine 1177 phosphorylation is not responsive to in vivo changes in shear stress.

Validation of the model by monitoring eNOS-GFP expression

Augmentation of shear stress up-regulates eNOS within 1 day, reaching a steady state after 2 days, which lasted until at least 6 days. These results are in agreement with previous findings.[13,14,21] Control experiments with a nontapered cast or the abolishment of shear stress in the tapered cast by blood flow arrest indicate that variations in local shear stress induce the observed responses in eNOS expression. Induction of oscillatory shear stress in the downstream area from the cast is demonstrated by Doppler sonography as well as by the loss of the alignment of endothelial cells with the flow direction. These results demonstrate that the new cast model is effective in triggering responses in gene expression caused by variations in shear stress.

The effects of shear stress on intracellular eNOS distribution

The correct intracellular localization of eNOS is of crucial importance for its activity.[23] By using eNOS mutants that were kinetically identical to unmodified eNOS, it was demonstrated that mislocalization of the enzyme impairs the production of NO in response to agonists.[24] Activation of eNOS by shear stress involves the Akt-dependent phosphorylation of eNOS at serine 1177.[18,25] It was recently shown that mainly the fraction of eNOS localized in the Golgi complex is responsive to phosphorylation by Akt.[20] Thus, the cellular distribution of eNOS in complex shear stress fields is essential for its function. To the best of our knowledge, the effect of

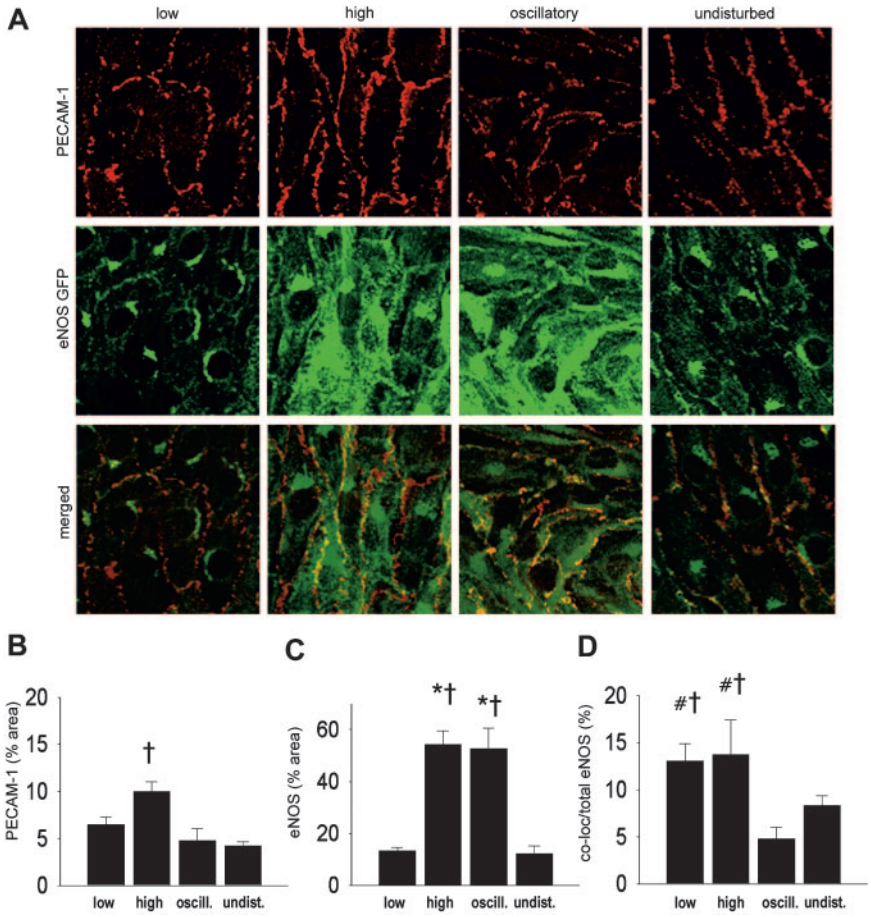

Figure 4. Intracellular localization of eNOS-GFP and PECAM-1 in regions of the carotid artery experiencing different shear stress patterns after 2 days of cast placement. (A) In the top panel, PECAM-1 in corresponding vascular regions visualized by *en face* immunofluorescence staining. Indicated are the low shear stress region (low), the high shear stress region (high), the oscillatory shear stress region (oscillatory), and the control region (undisturbed). Fluorescence was monitored by *en face* confocal microscopy in stacks of 500 × 500 × 40 μm each. In the middle panel, fluorescence of eNOS-GFP in endothelial cells located in the 3 different shear stress regions and in the contralateral carotid artery. In the bottom panel the top and middle panels are merged, showing the colocalization signal in yellow. (B-D) Quantification of the localization of (B) the PECAM-1, (C) the eNOS-GFP, and (D) the colocalization signals in response to the different shear stress fields in percentages of the total area (B-C) or of the total eNOS-GFP signal (D); n = 5, $*P < .05$ versus low shear stress. †$P < .05$ versus undisturbed shear stress. #$P < .05$ versus oscillatory shear stress. All data are means ± SEM.

shear stress on the intracellular redistribution of eNOS in endothelial cells has only been evaluated once in blood vessels in vivo.[26]

Our study shows that the Golgi complex becomes more extended in response to the augmentation of shear stress. This finding is in agreement with a previous study showing a difference in Golgi complex areas between venous endothelium (low shear stress) and arterial endothelium (high shear stress) in rats.[27] A significant part of eNOS bound to the plasma membrane is present at the cell-to-cell contact sites and colocalizes with PECAM-1.[27,28] We found that PECAM-1 itself is up-regulated under high shear stress. The relative distribution of eNOS to the PECAM-1$^+$ cell membrane region was not influenced by shear stress, indicating that intracellular eNOS and PECAM-1 increased to similar amounts in response to shear stress. In summary, our data show that both the cell membrane and the Golgi complex compartments of the eNOS pool are increased after augmenting shear stress.

In vitro studies demonstrated that phosphorylation of serine 1177 is responsive to shear stress.[29] Indeed, we found increased serine 1177 phosphorylation of eNOS under high and oscillatory shear stress conditions. It was recently demonstrated that the eNOS pool residing in the Golgi complex is more responsive to Akt phosphorylation of serine 1177 than eNOS residing in the cell membrane,[20] indicating that the shear stress–responsive eNOS pool is located predominantly in the Golgi complex. Rather unexpectedly, the relative fraction of eNOS located in the Golgi complex was unchanged in the low shear stress region but decreased in the high and oscillatory shear stress regions. The correlation found between Golgi complex area and total eNOS area (Figure 5) demonstrates a possible response by the endothelial cells to increase the size of the Golgi complex to accommodate more eNOS-GFP. When only the Golgi-localized eNOS fraction was taken into account, a similar correlation was found ($r^2 = 0.71$, $P < .001$). Therefore, we hypothesize that chronic changes in shear stress in vivo induce adaptations in the extension of the Golgi complex, enabling the endothelial cells to accommodate more eNOS protein in this shear stress–responsive intracellular compartment. This results in an absolute increase in eNOS phosphorylation and NO production, although the relative portion of eNOS that is phosphorylated remains unchanged.

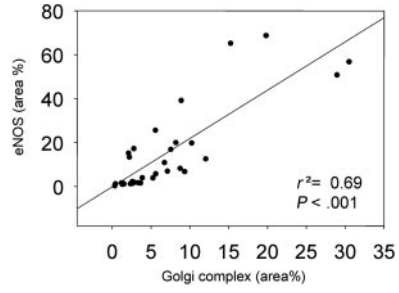

Figure 5. The correlation between the Golgi complex area versus eNOS-GFP area. Both are shown as a percentage of the total area.

Limitations of the study

mRNA studies. Although the fluorescent signal is clearly increased in the high shear stress region compared with the undisturbed shear stress region (middle panels in Figures 3A, 4A, and 6A), the eNOS mRNA levels were similar (Figure 2E). This could be due to differences in sampling. Confocal microscopy demonstrated significant variation in eNOS-GFP signal within the high shear stress region (Figure 2A). However, for RNA measurements complete segments

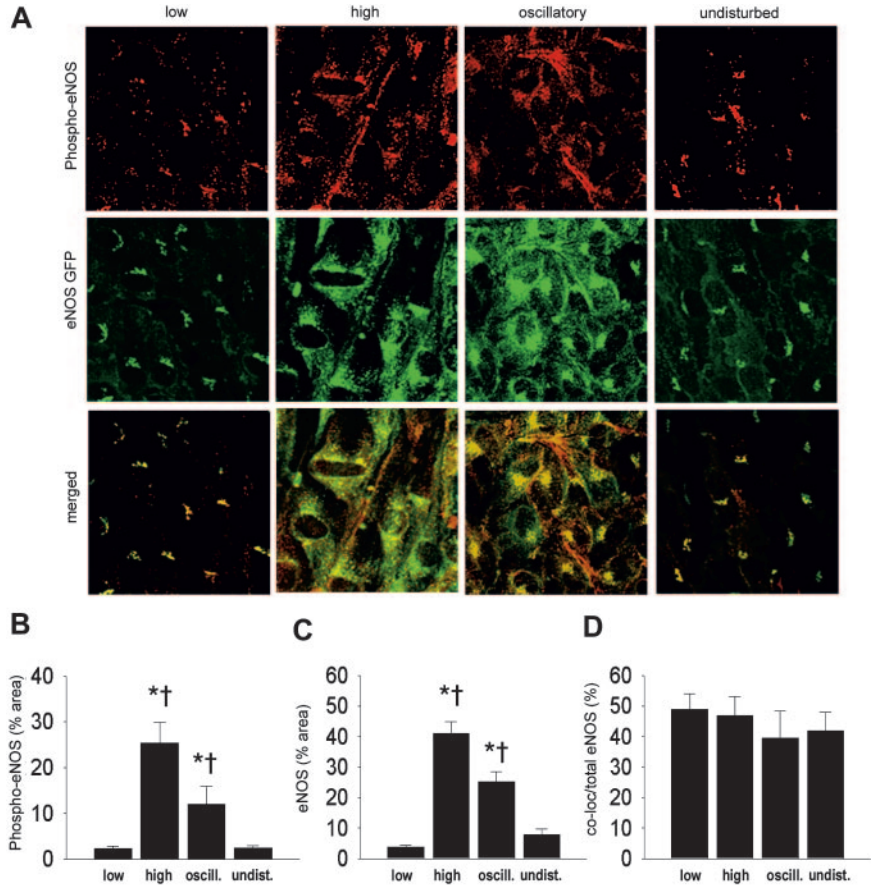

Figure 6. Intracellular localization of eNOS-GFP and phospho-eNOS in areas of the carotid artery experiencing different shear stress patterns after 2 days of cast placement. (A) In the top panel, phospho-eNOS in corresponding vascular regions visualized by *en face* immunofluorescence staining. Indicated are the low shear stress region (low), the high shear stress region (high), the oscillatory shear stress region (oscillatory), and the control region (undisturbed). Fluorescence was monitored by *en face* confocal microscopy in stacks of 500 × 500 μm each. In the middle panel, fluorescence of eNOS-GFP in endothelial cells located in the 3 different shear stress regions and in the contralateral carotid artery. In the bottom panel the top and middle panels are merged, showing the colocalization signal in yellow. (B-D) Quantification of the localization of (B) the phospho-eNOS, (C) the eNOS-GFP, and (D) the colocalization signals in response to the different shear stress fields in percentages of the total area (B-C) or of the total eNOS-GFP signal (D); n = 5, $*P < .05$ versus low shear stress. $\dagger P < .05$ versus undisturbed shear stress. All data are means ± SEM.

were collected and therefore the data represent the average eNOS expression, masking variations caused by hemodynamic differences within the segments. Part of the discrepancy might also be due to a posttranscriptional mechanism altering the half-life of eNOS mRNA.[13] When monitoring the expression of endogenous murine eNOS, we found responses in the 4 shear stress regions that were similar to those of eNOS-GFP (data not shown), supporting our findings.

Transgenic model. Overexpression of eNOS-GFP may result in a negative feedback by the increased NO production inhibiting transcription of the gene.[30] Thus, the effect of shear stress on eNOS expression might have been underestimated in the present study. However, the expression of murine eNOS in wild-type controls shows a similar response to the shear stress alterations induced by the cast. The observed effect of shear stress on eNOS-GFP is therefore not restricted to the human eNOS transgenic construct.

The GFP reporter might interfere with eNOS localization. eNOS myristoylation and palmitoylation, which are both important for the localization,[20] occur at the N-terminus. It is unlikely that these processes are affected because the GFP part is fused at the C-terminus of the eNOS protein.[15] Although GFP could induce changes in protein folding, our experiments show normal localization of eNOS-GFP in the Golgi complex and plasma membrane.[15] Previous studies extensively studied the location and function of the eNOS-GFP fusion protein in vitro.[27,28,31,32] These studies clearly indicate that the GFP moiety does not interfere with the localization and the function of eNOS.

The change in vessel geometry by cast placement may compress the fibroelastin layers of the vessel wall and thereby increase background autofluorescence. This does not affect our data, however, because the autofluorescent signal was subtracted from the total GFP signal. The tapering effect of the cast could also compress the endothelial cells to make them fit into a smaller area, increasing the number of cells per area. Colocalization studies of the endothelium in the different shear stress regions do not show an increase in cell number per area or a decrease in cell size. In addition, the up-regulation of eNOS-GFP in single endothelial cells is observed, providing further evidence that the eNOS-GFP signal in the high shear vessel segment is not an artifact created by the tapered shape of the cast.

In conclusion, the present study demonstrates that complex shear stress fields can be induced in straight vessels in vivo. Furthermore, novel information about the in vivo regulation of eNOS by shear stress can be obtained by using the cast model. This hemodynamic model provides, therefore, the opportunity to examine directly the effect of low, high, and oscillatory shear stress on the initiation and development of atherosclerotic disease.

References

1. Kamiya A, Togawa T. Adaptive regulation of wall shear stress to flow change in the canine carotid artery. Am J Physiol. 1980;H14–H21.
2. Kubis N, Checoury A, Tedgui A, Levy BI. Adaptive common carotid arteries remodeling after unilateral internal carotid artery occlusion in adult patients. Cardiovasc Res. 2001;50:597-602.
3. Caro CG, Fitz-Gerald JM, Schroter RC. Arterial wall shear and distribution of early atheroma in man. Nature. 1969;223:1159-1160.
4. VanderLaan PA, Reardon CA, Getz GS. Site specificity of atherosclerosis: site-selective responses to atherosclerotic modulators. Arterioscler Thromb Vasc Biol. 2004;24:12-22.
5. Gimbrone MA Jr. Vascular endothelium, hemodynamic forces, and atherogenesis. Am J Pathol. 1999;155:1-5.
6. Cooke JP. Flow, NO, and atherogenesis. Proc Natl Acad Sci U S A. 2003;100:768-770.
7. Stone PH, Coskun AU, Kinlay S, et al. Effect of

endothelial shear stress on the progression of coronary artery disease, vascular remodeling, and in-stent restenosis in humans: in vivo 6-month follow-up study. Circulation. 2003;108: 438-444.

8. Buchanan JR Jr, Kleinstreuer C, Truskey GA, Lei M. Relation between non-uniform hemodynamics and sites of altered permeability and lesion growth at the rabbit aorto-celiac junction. Atherosclerosis. 1999;143:27-40.
9. Shyy JY, Chien S. Role of integrins in endothelial mechanosensing of shear stress. Circ Res. 2002; 91:769-775.
10. Ohura N, Yamamoto K, Ichioka S, et al. Global analysis of shear stress-responsive genes in vascular endothelial cells. J Atheroscler Thromb. 2003;10:304-313.
11. Porat RM, Grunewald M, Globerman A, et al. Specific induction of tie1 promoter by disturbed flow in atherosclerosis-prone vascular niches and flow-obstructing pathologies. Circ Res. 2004;94:394-401.
12. Passerini AG, Polacek DC, Shi C, et al. Coexisting proinflammatory and antioxidative endothelial transcription profiles in a disturbed flow region of the adult porcine aorta. Proc Natl Acad Sci U S A. 2004;101:2482-2487.
13. Ziegler T, Silacci P, Harrison VJ, Hayoz D. Nitric oxide synthase expression in endothelial cells exposed to mechanical forces. Hypertension. 1998;32:351-355.
14. Tuttle JL, Nachreiner RD, Bhuller AS, et al. Shear level influences resistance artery remodeling: wall dimensions, cell density, and eNOS expression. Am J Physiol Heart Circ Physiol. 2001;218: H1380-H1389.
15. van Haperen R, Cheng C, Mees BM, et al. Functional expression of endothelial nitric oxide synthase fused to green fluorescent protein in transgenic mice. Am J Pathol. 2003;163:1677-1686.
16. Fulton D, Gratton JP, Sessa WC. Post-translational control of endothelial nitric oxide synthase: why isn't calcium/calmodulin enough? J Pharmacol Exp Ther. 2001;299:818-824.
17. Govers R, Rabelink TJ. Cellular regulation of endothelial nitric oxide synthase. Am J Physiol Renal Physiol. 2001;280:F193-F206.
18. Dimmeler S, Fleming I, Fisslthaler B, Hermann C, Busse R, Zeiher AM. Activation of nitric oxide synthase in endothelial cells by Akt-dependent phosphorylation. Nature. 1999;399:601-605.
19. Fisslthaler B, Dimmeler S, Hermann C, Busse R, Fleming I. Phosphorylation and activation of the endothelial nitric oxide synthase by fluid shear stress. Acta Physiol Scand. 2000;168:81-88.
20. Fulton D, Babbitt R, Zoellner S, et al. Targeting of endothelial nitric oxide synthase to the cytoplasmic face of the Golgi or plasma membrane regulates Akt- versus calcium-dependent mechanisms for nitric oxide release. J Biol Chem. 2004;279: 30349-30357.
21. Davis ME, Cai H, Drummond GR, Harrison DG. Shear stress regulates endothelial nitric oxide synthase expression through c-Src by divergent signaling pathways. Circ Res. 2001;89:1073-1080.
22. Wentzel JJ, Kloet J, Andhyiswara I, et al. Shear-stress and wall-stress regulation of vascular remodeling after balloon angioplasty: effect of matrix metalloproteinase inhibition. Circulation. 2001;104:91-96.
23. Shaul PW. Regulation of endothelial nitric oxide synthase: location, location, location. Annu Rev Physiol. 2002;64:749-774.
24. Garcia-Cardena G, Oh P, Liu J, Schnitzer JE, Sessa WC. Targeting of nitric oxide synthase to endothelial cell caveolae via palmitoylation: implications for nitric oxide signaling. Proc Natl Acad Sci U S A. 1996;93:6448-6453.
25. Fulton D, Gratton JP, McCabe TJ, et al. Regulation of endothelium-derived nitric oxide production by the protein kinase Akt. Nature. 1999;399: 597-601.
26. Rizzo V, McIntosh DP, Oh P, Schnitzer JE. In situ flow activates endothelial nitric oxide synthase in luminal caveolae of endothelium with rapid caveolin dissociation and calmodulin association. J Biol Chem. 1998;273:34724-34729.
27. Andries LJ, Brutsaert DL, Sys SU. Nonuniformity of endothelial constitutive nitric oxide synthase distribution in cardiac endothelium. Circ Res. 1998;82:195-203.
28. Govers R, Bevers L, de Bree P, Rabelink TJ. Endothelial nitric oxide synthase activity is linked to its presence at cell-cell contacts. Biochem J. 2002;361:193-201.
29. Rizzo V, Morton C, DePaola N, Schnitzer JE, Davies PF. Recruitment of endothelial caveolae into mechanotransduction pathways by flow conditioning in vitro. Am J Physiol Heart Circ Physiol. 2003;285:H1720-H1729.
30. Abu-Soud HM, Ichimori K, Presta A, Stuehr DJ. Electron transfer, oxygen binding, and nitric oxide feedback inhibition in endothelial nitric-oxide synthase. J Biol Chem. 2000;275:17349-17357.
31. Sowa G, Liu J, Papapetropoulos A, Rex-Haffner M, Hughes TE, Sessa WC. Trafficking of endothelial nitric-oxide synthase in living cells: quantitative evidence supporting the role of palmitoylation as a kinetic trapping mechanism limiting membrane diffusion. J Biol Chem. 1999;274: 22524-22531.
32. Liu J, Hughes TE, Sessa WC. The first 35 amino acids and fatty acylation sites determine the molecular targeting of endothelial nitric oxide synthase into the Golgi region of cells: a green fluorescent protein study. J Cell Biol. 1997;137:1525-1535.